Berry curvature dipole current in the transition metal dichalcogenides family

Jhih-Shih You,[1,2,*] Shiang Fang,[1,†] Su-Yang Xu,[3] Efthimios Kaxiras,[1,4] and Tony Low[5,‡]

[1]*Department of Physics, Harvard University, Cambridge, Massachusetts 02138, USA*
[2]*Institute for Theoretical Solid State Physics, IFW Dresden, Helmholtzstrasse 20, 01069 Dresden, Germany*
[3]*Department of Physics, Massachusetts Institute of Technology, Cambridge, Massachusetts 02139, USA*
[4]*John A. Paulson School of Engineering and Applied Sciences, Harvard University, Cambridge, Massachusetts 02138, USA*
[5]*Department of Electrical and Computer Engineering, University of Minnesota, Minneapolis, Minnesota 55455, USA*

We study the quantum nonlinear Hall effect in two-dimensional (2D) materials with time-reversal symmetry. When only one mirror line exists, a transverse charge current occurs in the second-order response to an external electric field, as a result of the Berry curvature dipole in momentum space. Candidate 2D materials to observe this effect are two-dimensional transition metal dichalcogenides (TMDCs). First, we use an *ab initio* based tight-binding approach to demonstrate that monolayer T_d-structure TMDCs exhibit a finite Berry curvature dipole. In the $1H$ and $1T'$ phase of TMDCs, we show the emergence of a finite Berry curvature dipole with the application of strain and an electrical displacement field, respectively.

Transition metal dichalcogenides (TMDCs) [1–4] have lately attracted considerable attention because of their rich physics, such as charge density waves [5–7], a superconducting phase [8], two-dimensional (2D) quantum spin Hall (QSH) states [9–13], and Weyl semimetal states [14], among other phenomena. Recently, numerous studies have demonstrated new physical properties in a monolayer (ML) of TMDCs that may be different from those in the bulk. For example, molybdenum disulfide (MoS_2) exhibits an induced indirect-to-direct band-gap transition from a $2H$ structure to its ML $1H$ structure, together with an enhancement of the luminescence quantum yield in comparison with the MoS_2 bulk [15,16]. The $1H$ structure which does not possess a center of inversion, in contrast to the $2H$ structure, allows optical control of the valley degrees of freedom [17].

Generally, the electronic properties of monolayer TMDCs with a chemical composition MX_2 ($M =$ Mo, W and $X =$ S, Se, Te) are directly related to their crystal structure, which includes the $1H$ ($P\bar{6}m2$), $1T$ ($P\bar{3}m2$), $1T'$ ($P2_1/m$), and T_d ($P1m1$) crystal structures, shown in Fig. 1. $1H$-MX_2 is a semiconductor with a direct band gap in the range of visible light (1–2 eV) [1,18,19] and the $1T$ structure is metallic [20]. Topological phases occur in $1T'$ structures since the global properties of electronic wave functions exhibit a nontrivial topology, theoretically predicted [9] and experimentally confirmed [10–13] to be a 2D quantum spin Hall state.

The local curvature of the wave function, defined as the Berry curvature (BC) [21,22], is a geometrical property of the Bloch energy band. The finite Berry curvature reveals a linear response, such as anomalous Hall conductivity [21],

and a nonlinear response, such as the circular photogalvanic effect (CPGE) and the nonlinear Hall effect [23–34]. In TMDCs, the BC at the two valleys takes opposite values, giving rise to bulk topological charge neutral valley current [35–37], as a linear response. For a nonlinear response, the semiclassical approach has been used to describe the intraband contributions to transverse current at both zero frequency and second harmonic generation in terms of the dipole moment of the BC in momentum space [26]. In the dc limit, the photocurrent can remain finite as a transverse Hall-like current [26,32].

In this Rapid Communication, we study the emergence of the nonlinear Hall current induced by the BC dipole in various 2D TMDC structures, using *ab initio* calculations combined with a semiclassical approach. Monolayer TMDCs with low crystalline symmetry are expected to be excellent candidates for observing these quantum nonlinear effects [26]. Our study quantitatively reveals the finite BC dipole in the T_d-structure monolayer TMDCs, where only one mirror line survives. For the $1H$ structure, uniaxial strain can break the underlying C_{3v} symmetry which otherwise ensures a vanishing nonlinear response. In addition, we evaluate the Berry dipole of strained TMDC. Lastly, we show that application of an out-of-plane electrical displacement field induces a strong BC dipole which is absent in $1T'$ monolayer TMDCs. Our results represent a numerical demonstration of nonlinear current in 2D TMDCs, which can be controlled by mechanical and/or electrical means. The proposed strategies of a tunable BC dipole also apply to a wide range of other two-dimensional materials, such as hexagonal boron nitride [38] and black phosphorus [39–41].

In the presence of an external electric field, the carrier velocity contains contributions from the group velocity of the electron wave and from the anomalous transverse term due to the BC, given by $-\frac{e}{\hbar}\vec{E} \times \Omega_z^{(n)}(\vec{k})$. Here, the BC for the electronic Bloch states of the nth band is defined

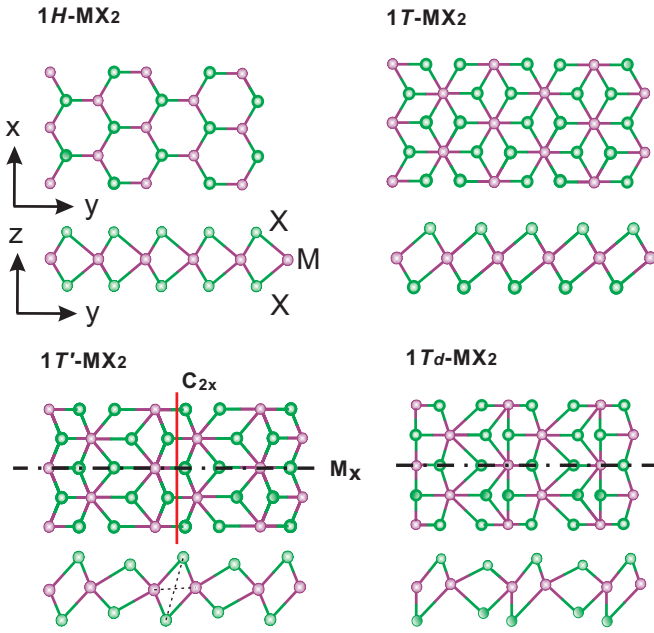*jhihshihyou@gmail.com
†shiangfang913@gmail.com
‡tlow@umn.edu

1H-MX₂

1T-MX₂

1T′-MX₂

1Td-MX₂

FIG. 1. Crystal structures of $1H$, $1T$, $1T'$, and $1T_d$ monolayer transition metal dichalcogenides MX_2 (M = Mo, W and X = S, Se, Te). The red solid line represents a screw rotate symmetry C_{2x} axis which involves a 180° rotation about $\hat{x}$ and a half lattice-constant translation along $\hat{x}$. The dashed-dotted line represents the mirror symmetry M_x. The combination of C_{2x} and M_x symmetries leads to the inversion symmetry for the $1T'$ structure. The $1T_d$ phase has only M_x symmetry.

as [22,42,43]

$$\Omega_z^{(n)}(\vec{k}) = i\hat{z} \cdot \left(\nabla_{\vec{k}} u_{\vec{k}}^{(n)*}\right) \times \left(\nabla_{\vec{k}} u_{\vec{k}}^{(n)}\right) \tag{1}$$

$$= -2\left(\frac{\hbar}{e}\right)^2 \sum_{n \neq n'} \frac{\text{Im}\langle u_{\vec{k}}^{(n)}|P_x(\vec{k})|u_{\vec{k}}^{(n')}\rangle\langle u_{\vec{k}}^{(n')}|P_y(\vec{k})|u_{\vec{k}}^{(n)}\rangle}{\left[\epsilon_{\vec{k}}^{(n)} - \epsilon_{\vec{k}}^{(n')}\right]^2}, \tag{2}$$

where $\epsilon_{\vec{k}}^{(n)}$ and $|u_{\vec{k}}^{(n)}\rangle$ are eigenvalues and eigenfunctions of the Hamiltonian $\hat{H}_{\vec{k}}$, respectively, at the momentum $\vec{k}$ and $P_i(\vec{k}) = (e/\hbar)\partial\hat{H}_{\vec{k}}/\partial k_i$ is the current operator. The BC is analogous to an effective magnetic field in the momentum space. Within linear response theory, the integral of the BC over the entire Brillouin zone gives rise to a transverse conductivity, which is simply given by $\sigma_{xy,n} = e^2/\hbar \int d^2\vec{k} f_0^{(n)}(\vec{k})\Omega_z^{(n)}(\vec{k})$, where $f_0^{(n)}(\vec{k})$ is the equilibrium Fermi-Dirac distribution function for the nth band. The transverse conductivity is zero for a time-reversal-invariant system, since states at $\vec{k}$ and $-\vec{k}$ are equally occupied and time-reversal symmetry requires that $\Omega_z^{(n)}(\vec{k}) = -\Omega_z^{(n)}(-\vec{k})$. When the system is driven out of equilibrium, a net transverse current can survive as the second-order response to the electric field. The combination of time-reversal (TR) and inversion symmetry restricts $\Omega_z^{(n)}(\vec{k}) = 0$ over the entire Brillouin zone. Thus, for a TR-invariant system, inversion symmetry breaking is necessary to generate a finite BC.

We first examine the nature of the nonlinear current with a symmetry analysis. In the presence of a driving in-plane electric field, $E_k = \text{Re}\{\mathcal{E}_k e^{i\omega t}\}$, the nonlinear current is written as $j_i = j_i^{(0)} + j_i^{(2\omega)} e^{2i\omega t}$, where the dc and second harmonic generated currents are described by the second-order susceptibility tensor as $j_i^{(0)} = \chi_{ijk}\mathcal{E}_j^*\mathcal{E}_k$ and $j_i^{(2\omega)} = \chi_{ijk}\mathcal{E}_j\mathcal{E}_k$, respectively. The tensor indices i, j, k span the 2D sample coordinates x, y. χ_{ijk} respects the symmetry of the crystal lattice. The presence of M_x mirror symmetry forces χ_{ijk} to be zero if any χ_{ijk} contains an odd number of the index x. All tensor components identically vanish in the presence of inversion symmetry. Thus, for a crystal breaking inversion but preserving the mirror symmetry M_x, $\chi_{yxx} \neq 0$, demonstrating that a Hall-like transverse current can occur in a second-order response to an external electric field $\mathcal{E}_x$.

The expression of nonlinear currents has been theoretically obtained within the semiclassical Boltzmann transport theory for a single band [25,26]. Up to second order in the driving electric field, previous theoretical works showed that in the case involving only the intraband process, a nonlinear Hall-like current density is expressed as

$$\vec{j}^{(0)} = \frac{e^3\tau}{2\hbar^2(1 + i\omega\tau)}\hat{z} \times \vec{\mathcal{E}}^*(D \cdot \vec{\mathcal{E}}), \tag{3}$$

$$\vec{j}^{(2\omega)} = \frac{e^3\tau}{2\hbar^2(1 + i\omega\tau)}\hat{z} \times \vec{\mathcal{E}}(D \cdot \vec{\mathcal{E}}), \tag{4}$$

with

$$D_i = \sum_n \int d^2\vec{k} f_0^{(n)}(\vec{k})\left[\partial_{k_i}\Omega_z^{(n)}(\vec{k})\right]$$

$$= -\sum_n \int d^2\vec{k}\left[\partial_{k_i} f_0^{(n)}(\vec{k})\right]\Omega_z^{(n)}(\vec{k}), \tag{5}$$

where τ is the relaxation time. The nonlinear dc current is proportional to the dipole moment of the BC over the occupied states. In fact, according to Eq. (5), the nonlinearity of these currents is associated with a "Fermi-surface" contribution, that is, only states near the Fermi surface can contribute to the integral in the low-temperature limit. The largest symmetry of a 2D crystal that allows for a nonvanishing BC dipole is a single mirror line [26]. Combining Eq. (5) with the fact that $\Omega_z^{(n)}(k_x, k_y) = -\Omega_z^{(n)}(-k_x, k_y)$ enforced by the mirror plane M_x, it is evident that $D_x \neq 0$ and $D_y = 0$. In what follows, we obtain D_x and D_y in units of Å. Consequently, according to Eqs. (3) and (4), when the driving electric field $E_k(t) = \mathcal{E}_k$ is aligned with the direction of the Berry curvature dipole vector D_x, we obtain the dc current density $j = 2j^{(0)} = 3698.1$ (A/m²) $\times D_x \sim 10^{-7}$ (A/m), where we choose $\tau = 10^{-12}$ s, $D_x = 1$ Å, and $\mathcal{E}_x = 100$ V/m.

The BC dipole is tied to the underlying crystal structure of monolayer TMDC. The most studied polymorphic structures of pristine monolayer TMDCs are $1H$, $1T$, and $1T'$ [44,45], shown in Fig. 1. The energetically favorable $1H$-MX_2 layer is built from two hexagonal lattices of X atoms and an intercalated hexagonal plane of M atoms forming a simple ABA Bernal stacking with $P\bar{6}m2$ space-group symmetry. In a monolayer unit of H structure, the inversion symmetry is explicitly broken. The lack of an inversion center in TMDCs produces substantial local BCs near the K, K' valleys. Due to time-reversal symmetry, the curvature at the two valleys has

opposite sign, which implies counterpropagating currents that persist even when the system is in equilibrium. Due to exact cancellation from the two valleys, these transverse currents are charge neutral to a linear response in an applied external electric field. The nonlinear contribution could still exist when the samples have just one mirror symmetry. The 2D materials such as monolayer TMDCs in the H structure do not have currents in a nonlinear response to the electric field because their C_{3v} symmetry forces the BC dipole to vanish.

The $1T\text{-}MX_2$ layer forms a rhombohedral ABC stacking phase with $P\bar{3}m2$ space group. In this structure, the transition metal atoms are octahedrally coordinated. Density functional theory (DFT) calculations show that the free-standing $1T$ structure is typically unstable and undergoes a Peierls distortion in one direction to form a 2×1 reconstruction, where the distorted M atoms form one-dimensional (1D) zigzag chains [46], referred to as the T' structure. Inversion symmetry is present in both the T and T' structure. The inversion-symmetric $1T'$ structure consists of two independent symmetries, the mirror symmetry M_x and the twofold screw rotational symmetry C_{2x}. Due to the inversion symmetry and time-reversal symmetry, $\Omega_z^{(n)}(\vec{k}) = 0$ over the entire Brillouin zone for the $1T'$ structure.

A candidate material to observe the quantum nonlinear Hall effect is monolayer WTe$_2$, whose structure T_d deviates slightly from the widely studied $1T'$ structure. In the T_d phase, the M_x mirror symmetry is preserved but the C_{2x} symmetry is weakly broken. As a result, the T_d structure with symmetry space group $P1m1$ actually breaks inversion symmetry and allows a nonzero BC dipole to exist. We perform *ab initio* DFT calculations using the Vienna *ab initio* simulation package (VASP) [47,48] with a minimal basis based on a transformation of the Kohn-Sham density functional theory Hamiltonian to a basis of maximally localized Wannier functions [49] as implemented in the WANNIER90 code. A slab geometry is employed to model single or double layers with a 20-Å vacuum region between periodic images to minimize the interaction between slabs. For TMDC materials, the relevant states consist of seven valence bands and four conduction bands, which are hybrids of metal d orbitals and chalcogen p orbitals. Therefore, the Wannier projections to the p/d orbitals provide us the *ab initio* tight-binding Hamiltonian for computing the BC dipole [50,51].

In Fig. 2 we shows that the ML WTe$_2$ with spin-orbit coupling (SOC) exhibits a finite BC dipole. The SOC leads to an inverted, indirect quantum spin Hall gap. In the DFT calculation, we used the Heyd-Scuseria-Ernzerhof (HSE) method [52] with the hybrid parameter set at HSE = 0.4, which gives a global band gap of 50 meV. In the vicinity of the gap minimum, the BC for the lowest conduction band exhibits two hot spots of opposite sign, as shown in Fig. 2(c). Such a bipolar configuration of BC is due to the M_x symmetry. It is worth noting that the distribution of BC near each hot spot is not uniform, leading to a nonzero BC dipole. To better understand the physics, we rewrite Eq. (5) as $D_x = \sum_n \int d^2\vec{k}\,\delta(\epsilon_{\vec{k}}^{(n)} - E_F)[\partial_{k_x}\epsilon_{\vec{k}}^{(n)}]\Omega_z^{(n)}(\vec{k})$, where E_F is the Fermi energy and $\partial_{k_x}\epsilon_{\vec{k}}^{(n)}$ is associated with the velocity along the x direction. Let us first consider the case of one Dirac cone (one hot spot). If the BC is constant and the
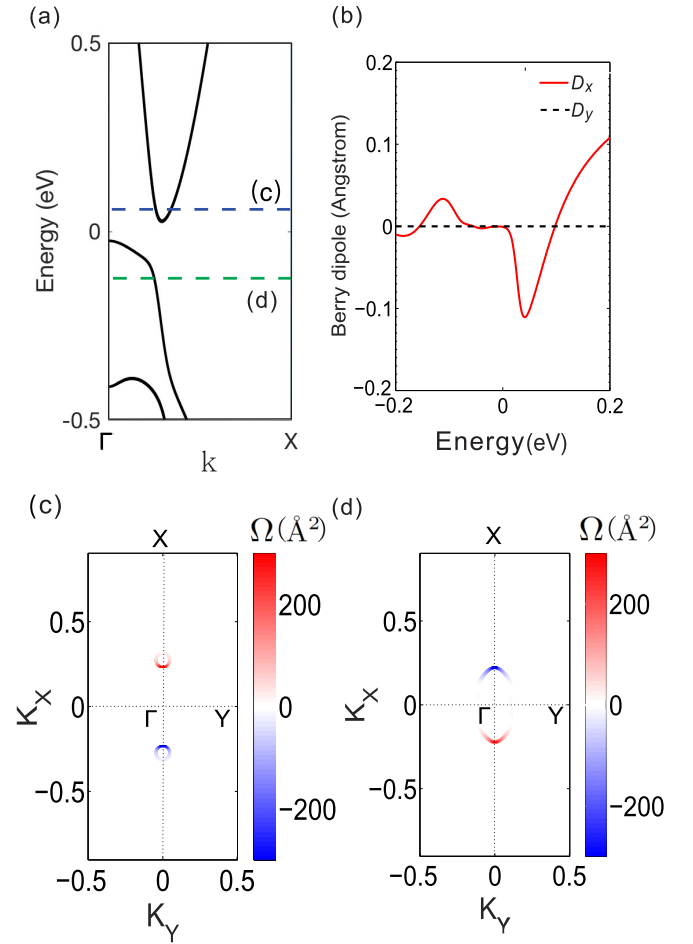

FIG. 2. (a) Band structure along Γ-X for the monolayer T_d-structure WTe$_2$. The global band gap is around 0.05 eV. The weak inversion breaking induces a tiny spin splitting near the bottom of the conduction band. The blue and green dashed lines correspond to 0.05 and -0.1 eV at which the Berry curvature is shown in (c) and (d), respectively. (b) Berry curvature dipole D_x and D_y. (c) and (d) Berry curvature at 0.05 and -0.1 eV, respectively.

velocity is equal but opposite around a perfect Dirac cone, the BC dipole will vanish. However, for a tilted Dirac cone which has anisotropic BC and velocity around E_F, a finite BC dipole is allowed. In Fig. 2(c), the red (blue) hot spot shows more intense positive (negative) BC in the left (right) part of the Dirac cone, where the velocity is negative (positive) along the x direction, leading to a negative BC dipole. For the highest valence band, the slope is negative along Γ to X, as shown in Fig. 2(a). Thus, the configuration of BC in Fig. 2(d) gives a positive BC dipole.

The H-structure monolayer TMDCs do not have nonlinear currents due to their C_{3v} symmetry, but applying uniaxial strain can reduce this symmetry, leaving only a single mirror operation, in which case the quantum nonlinear Hall effect can be observed [26]. The application of strain transforms the vector $\vec{r}_0$, which denotes an undistorted crystal coordinate, into the new position $\vec{r} = \vec{r}_0 + \vec{u}$, where $\vec{r}_0 = (x, y)$ and $\vec{u} = [u_x(x, y), u_y(x, y)]$ are the position and displacement deformation vector fields, respectively. Here, we are con-
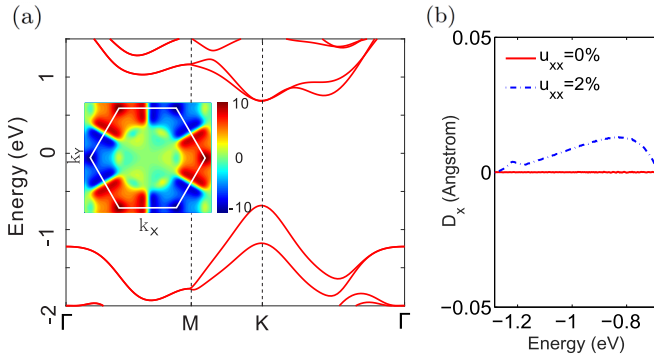
FIG. 3. (a) Band structure along Γ-M-K-Γ for the unstrained H-structure WSe$_2$; the inset shows the Berry curvature contributed from the top two valence bands. The Brillouin zone is presented in the white solid line. (b) Berry curvature dipole D_x of the monolayer H-structure WSe$_2$ with strain $u_{xx} = 0$ (red line) and $u_{xx} = 2\%$ (blue dotted line) when $u_{yy} = u_{xy} = 0$. $D_y = 0$ for all strains.

sidering only the acoustic part of the in-plane displacement vector. In general, the derivative of $\vec{u}$ can be decomposed as $\vec{\nabla} \vec{u} = \varepsilon + \omega$, where ε and ω are the strain and rotation tensors, respectively.

The simplest way to incorporate the effect of strain is to vary the interatomic bond lengths $|\delta_{\alpha\beta}|$ between the α and β sites, which is known as the central force approximation. At the linear order and under this approximation, the modified hopping terms in the presence of strain can be approximated as

$$ t_{\alpha\beta} = t^0_{\alpha\beta} + \mu \vec{\delta}_{\alpha\beta} \cdot (\vec{\delta}_{\alpha\beta} \cdot \vec{\nabla}) \vec{u}, \quad \mu = \frac{1}{|\delta_{\alpha\beta}|} \left[\frac{dt_{\alpha\beta}}{d|\delta_{\alpha\beta}|} \right]. \quad (6) $$

The central force approximation fails to capture the change in the hopping when the crystal is stretched along a direction perpendicular to the bond. The microscopic models based on the *ab initio* derived Wannier functions describe up to linear order contributions in the strain $(u_{xx} + u_{yy})$, $(u_{xx} - u_{yy})$, and u_{xy} with respect to the crystal symmetry and local crystal configuration, free from any empirical fitting procedures.

Based on the models of strained TMDCs [53], the BC dipole can be readily evaluated. Figure 3 shows that the H-structure WSe$_2$ with strain exhibits the BC dipole. The Brillouin zone of monolayer TMDC with Dirac points is shifted away from the K and K' by uniaxial strain. When the shear strain is applied along high-symmetry lines, one obtains finite D_x but zero D_y.

The application of an out-of-plane electrical displacement field can be used to systematically control the magnitude of the nonlinear Hall current. This can be understood from a third-order susceptibility tensor $\chi^{(3)}_{ijjz}$. In the presence of a static electrical displacement field $\mathcal{E}_{d,z}$ along the z direction, the nonlinear dc current is written as $j_i^{(0)} = \chi^{(2)}_{ijj} |\mathcal{E}_j|^2 + \chi^{(3)}_{ijjz} |\mathcal{E}_j|^2 \mathcal{E}_{d,z}$. We obtain the effective second-order tensor containing the electrical displacement field effect as $\tilde{\chi}^{(2)}_{ijj} \equiv \chi^{(2)}_{ijj} + \chi^{(3)}_{ijjz} \mathcal{E}_{d,z}$. When $\chi^{(2)}_{ijj} = 0$ due to the intrinsic inversion symmetry, $\mathcal{E}_{d,z}$ makes it possible to produce the second response with a significant amplitude.
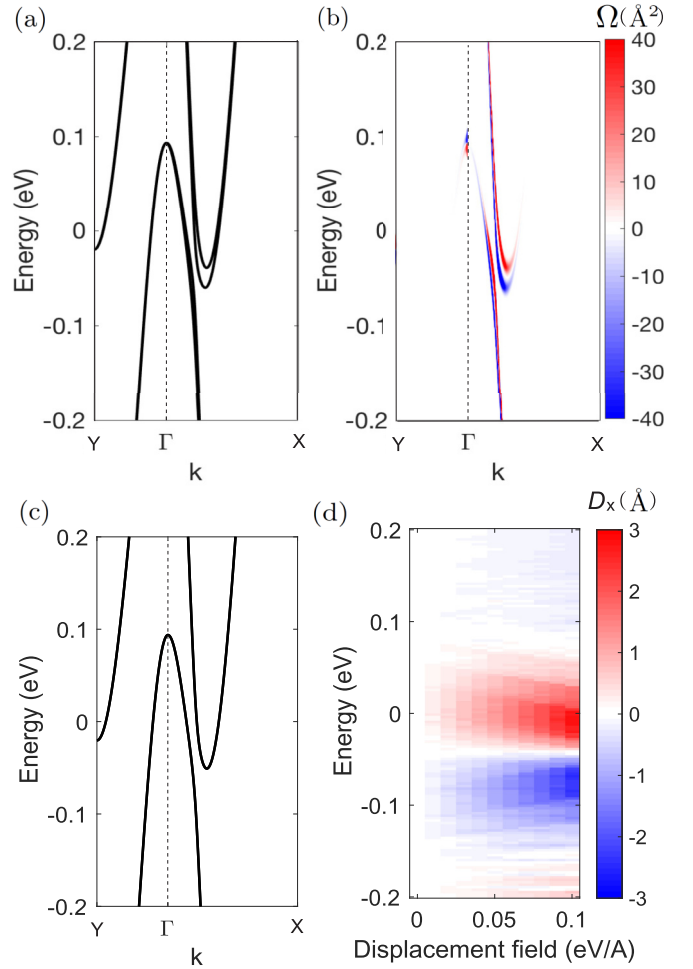

FIG. 4. (a) Band structure and (b) Berry curvature $\Omega^{(n)}_z(\vec{k})$ along Y-Γ-X for the ML $1T'$-structure MoTe$_2$ at $\mathcal{E}_{d,z} = 0.06$ eV/Å. (c) Band structure at $\mathcal{E}_{d,z} = 0$. The BC is zero at all energies due to the presence of inversion symmetry. (d) BC dipole D_x induced by the electrical displacement field (eV/Å) in the z direction which breaks the inversion symmetry. $D_y = 0$ in all cases.

Finally, we consider the basic symmetry properties of the Hamiltonian for the TMDC family of materials in the presence of $\mathcal{E}_{d,z}$. The $1T'$ phase has inversion symmetry from the combination of twofold screw rotational symmetry C_{2x} and the mirror symmetry M_x. Therefore the monolayer $1T'$ structure, which has zero BC dipole, can acquire a nonzero dipole if $\mathcal{E}_{d,z}$ is applied to break the C_{2x} symmetry and thus inversion symmetry. This inversion symmetry-breaking scheme can be simply modeled with only an electrostatic on-site potential within each unit cell. We show the monolayer MoTe$_2$ with $1T'$ structure as a function of the electrical displacement $\mathcal{E}$ field in the z direction in Fig. 4. The enhancement of the BC dipole is evident. This illustrates how to control and modulate the BC dipole with an external field.

In conclusion, we discussed the nonlinear current induced by the BC dipole in 2D materials of the TMDC family. The existence of only a single mirror symmetry line is needed to provide a finite BC dipole. Breaking of the crystal symmetry can be controlled by mechanical and/or electrical means.

Certainly, it would be desirable to explore if the proposed effect could be observed in other 2D materials subject to the same symmetry constraints. Such a tunable BC dipole can not only lead to the quantum nonlinear Hall effect but could also be relevant for the understanding of other quantum geometrical phenomena.

Note added. Recently, we became aware of an independent work by Zhang *et al.* [54] which also shows the nonlinear electric response in $MoTe_2$ and WTe_2 monolayers.

[1] B. Radisavljevic, A. Radenovic, J. Brivio, V. Giacometti, and A. Kis, Nat. Nanotechnol. **6**, 147 (2011).

[2] Q. H. Wang, K. Kalantar-Zadeh, A. Kis, J. N. Coleman, and M. S. Strano, Nat. Nanotechnol. **7**, 699 (2012).

[3] A. K. Geim and I. V. Grigorieva, Nature (London) **499**, 419 (2013).

[4] S. Z. Butler, S. M. Hollen, L. Cao, Y. Cui, J. A. Gupta, H. R. Gutiérrez, T. F. Heinz, S. S. Hong, J. Huang, A. F. Ismach, E. Johnston-Halperin, M. Kuno, V. V. Plashnitsa, R. D. Robinson, R. S. Ruoff, S. Salahuddin, J. Shan, L. Shi, M. G. Spencer, M. Terrones *et al.*, ACS Nano **7**, 2898 (2013).

[5] J. A. Wilson, F. J. D. Salvo, and S. Mahajan, Adv. Phys. **50**, 1171 (2001).

[6] T. Ritschel, J. Trinckauf, K. Koepernik, B. Büchner, M. v. Zimmermann, H. Berger, Y. I. Joe, P. Abbamonte, and J. Geck, Nat. Phys. **11**, 328 (2015).

[7] A. W. Tsen, R. Hovden, D. Wang, Y. D. Kim, J. Okamoto, K. A. Spoth, Y. Liu, W. Lu, Y. Sun, J. C. Hone, L. F. Kourkoutis, P. Kim, and A. N. Pasupathy, Proc. Natl. Acad. Sci. USA **112**, 15054 (2015).

[8] J. T. Ye, Y. J. Zhang, R. Akashi, M. S. Bahramy, R. Arita, and Y. Iwasa, Science **338**, 1193 (2012).

[9] X. Qian, J. Liu, L. Fu, and J. Li, Science **346**, 1344 (2014).

[10] Z. Fei, T. Palomaki, S. Wu, W. Zhao, X. Cai, B. Sun, P. Nguyen, J. Finney, X. Xu, and D. H. Cobden, Nat. Phys. **13**, 677 (2017).

[11] S. Tang, C. Zhang, D. Wong, Z. Pedramrazi, H.-Z. Tsai, C. Jia, B. Moritz, M. Claassen, H. Ryu, S. Kahn, J. Jiang, H. Yan, M. Hashimoto, D. Lu, R. G. Moore, C.-C. Hwang, C. Hwang, Z. Hussain, Y. Chen, M. M. Ugeda *et al.*, Nat. Phys. **13**, 683 (2017).

[12] Z.-Y. Jia, Y.-H. Song, X.-B. Li, K. Ran, P. Lu, H.-J. Zheng, X.-Y. Zhu, Z.-Q. Shi, J. Sun, J. Wen, D. Xing, and S.-C. Li, Phys. Rev. B **96**, 041108 (2017).

[13] S. Wu, V. Fatemi, Q. D. Gibson, K. Watanabe, T. Taniguchi, R. J. Cava, and P. Jarillo-Herrero, Science **359**, 76 (2018).

[14] A. A. Soluyanov, D. Gresch, Z. Wang, Q. Wu, M. Troyer, X. Dai, and B. A. Bernevig, Nature (London) **527**, 495 (2015).

[15] A. Splendiani, L. Sun, Y. Zhang, T. Li, J. Kim, C.-Y. Chim, G. Galli, and F. Wang, Nano Lett. **10**, 1271 (2010).

[16] K. F. Mak, C. Lee, J. Hone, J. Shan, and T. F. Heinz, Phys. Rev. Lett. **105**, 136805 (2010).

[17] H. Zeng, J. Dai, W. Yao, D. Xiao, and X. Cui, Nat. Nanotechnol. **7**, 490 (2012).

[18] X. R. Qin, D. Yang, R. F. Frindt, and J. C. Irwin, Phys. Rev. B **44**, 3490 (1991).

[19] S. Fang, R. Kuate Defo, S. N. Shirodkar, S. Lieu, G. A. Tritsaris, and E. Kaxiras, Phys. Rev. B **92**, 205108 (2015).

[20] R. Kappera, D. Voiry, S. E. Yalcin, W. Jen, M. Acerce, S. Torrel, B. Branch, S. Lei, W. Chen, S. Najmaei, J. Lou, P. M. Ajayan, G. Gupta, A. D. Mohite, and M. Chhowalla, APL Mater. **2**, 092516 (2014).

[21] N. Nagaosa, J. Sinova, S. Onoda, A. H. MacDonald, and N. P. Ong, Rev. Mod. Phys. **82**, 1539 (2010).

[22] D. Xiao, M.-C. Chang, and Q. Niu, Rev. Mod. Phys. **82**, 1959 (2010).

[23] E. Deyo, L. E. Golub, E. L. Ivchenko, and B. Spivak, arXiv:0904.1917.

[24] J. E. Moore and J. Orenstein, Phys. Rev. Lett. **105**, 026805 (2010).

[25] T. Low, Y. Jiang, and F. Guinea, Phys. Rev. B **92**, 235447 (2015).

[26] I. Sodemann and L. Fu, Phys. Rev. Lett. **115**, 216806 (2015).

[27] M. Eginligil, B. Cao, Z. Wang, X. Shen, C. Cong, J. Shang, C. Soci, and T. Yu, Nat. Commun. **6**, 7636 (2015).

[28] F. de Juan, A. G. Grushin, T. Morimoto, and J. E. Moore, Nat. Commun. **8**, 15995 (2017).

[29] S. S. Tsirkin, P. A. Puente, and I. Souza, Phys. Rev. B **97**, 035158 (2018).

[30] Y. Zhang, Y. Sun, and B. Yan, Phys. Rev. B **97**, 041101 (2018).

[31] J. Quereda, T. S. Ghiasi, J.-S. You, J. van den Brink, B. J. van Wees, and C. H. van der Wal, Nat. Commun. **9**, 3346 (2018).

[32] S.-Y. Xu, Q. Ma, H. Shen, V. Fatemi, S. Wu, T.-R. Chang, G. Chang, A. M. M. Valdivia, C.-K. Chan, Q. D. Gibson, J. Zhou, Z. Liu, K. Watanabe, T. Taniguchi, H. Lin, R. J. Cava, L. Fu, N. Gedik, and P. Jarillo-Herrero, Nat. Phys. **14**, 900 (2018).

[33] J. I. Facio, D. Efremov, K. Koepernik, J.-S. You, I. Sodemann, and J. van den Brink, arXiv:1805.02680.

[34] L.-k. Shi and J. C. W. Song, arXiv:1805.00939.

[35] D. Xiao, G.-B. Liu, W. Feng, X. Xu, and W. Yao, Phys. Rev. Lett. **108**, 196802 (2012).

[36] K. F. Mak, K. L. McGill, J. Park, and P. L. McEuen, Science **344**, 1489 (2014).

[37] Y. D. Lensky, J. C. W. Song, P. Samutpraphoot, and L. S. Levitov, Phys. Rev. Lett. **114**, 256601 (2015).

[38] D. Golberg, Y. Bando, Y. Huang, T. Terao, M. Mitome, C. Tang, and C. Zhi, ACS Nano **4**, 2979 (2010).

[39] A. Morita, Appl. Phys. A: Solids Surf. **39**, 227 (1986).

[40] L. Li, Y. Yu, G. J. Ye, Q. Ge, X. Ou, H. Wu, D. Feng, X. H. Chen, and Y. Zhang, Nat. Nanotechnol. **9**, 372 (2014).

[41] H. Liu, A. T. Neal, Z. Zhu, Z. Luo, X. Xu, D. Tománek, and P. D. Ye, ACS Nano **8**, 4033 (2014).

[42] J. N. Fuchs, F. Piéchon, M. O. Goerbig, and G. Montambaux, Eur. Phys. J. B **77**, 351 (2010).

[43] X. Xu, W. Yao, D. Xiao, and T. F. Heinz, Nat. Phys. **10**, 343 (2014).

[44] J. Heising and M. G. Kanatzidis, J. Am. Chem. Soc. **121**, 11720 (1999).

[45] G. Eda, T. Fujita, H. Yamaguchi, D. Voiry, M. Chen, and M. Chhowalla, ACS Nano **6**, 7311 (2012).

[46] M. Kan, J. Y. Wang, X. W. Li, S. H. Zhang, Y. W. Li, Y. Kawazoe, Q. Sun, and P. Jena, J. Phys. Chem. C **118**, 1515 (2014).

[47] G. Kresse and J. Furthmüller, Phys. Rev. B **54**, 11169 (1996).

[48] G. Kresse and J. Furthmller, Comput. Mater. Sci. **6**, 15 (1996).

[49] A. A. Mostofi, J. R. Yates, Y.-S. Lee, I. Souza, D. Vanderbilt, and N. Marzari, Comput. Mater. Sci. **178**, 685 (2008).

[50] T. Fukui, Y. Hatsugai, and H. Suzuki, J. Phys. Soc. Jpn. **74**, 1674 (2005).

[51] Based on the tight-binding Hamiltonian, the BC is computed in the discretized Brillouin zone [50]. For the BC dipole, we sample the first Brillouin zone more than $500 \times 500k$ grids.

[52] J. Heyd, G. E. Scuseria, and M. Ernzerhof, J. Chem. Phys. **118**, 8207 (2003).

[53] S. Fang, S. Carr, M. A. Cazalilla, and E. Kaxiras, Phys. Rev. B **98**, 075106 (2018).

[54] Y. Zhang, J. van den Brink, C. Felser, and B. Yan, arXiv:1804.11069.